Electrochemical characteristics of $Ca_2Na_{n-3}Nb_nO_{3n+1}$/PEDOT:PSS hybrid electrodes for environmentally friendly solar water splitting

Electrochemical characteristics of $Ca_2Na_{n-3}Nb_nO_{3n+1}$/PEDOT:PSS hybrid electrodes for environmentally friendly solar water splitting

M R Aziza[1,*], N A Hasanah[1], A Junikhah[1], K A Wibowo[1], A A Nurpratiwi[2], C W Chang[2], Y H Su[2]

[1] Department of Electrical Engineering, UIN Maulana Malik Ibrahim Malang, Malang, Indonesia
[2] Department of Materials Science and Engineering, National Cheng-Kung University, Tainan, Taiwan

[*]E-mail: miladinarizka@uin-malang.ac.id

Abstract. The development of functional electrode materials that combine efficient charge transport with high electrochemical activity is critical for advancing integrated energy devices. In this study, we investigate the electrochemical characteristics of $Ca_2Na_{n-1}Nb_nO_{3n+1}$/PEDOT:PSS (n = 4, 5, 6) hybrid electrodes, which focus on their suitability for solar water splitting application. $Ca_2Na_{n-1}Nb_nO_{3n+1}$ (CNNO) nanosheets were obtained via mechanical exfoliation from bulk $KCa_2Na_{n-1}Nb_nO_{3n+1}$ (KCNNO) materials and subsequently mixed with PEDOT:PSS to form P-N junction. The resulting CNNO/PEDOT:PSS dispersion was then drop-cast onto ITO glass substrates for performance evaluation. Cyclic voltammetry (CV) analysis reveals that CNNO5/PEDOT:PSS exhibits the best CV performance, which reflects its enhanced charge storage and redox acitivity. However, electrochemical impedance spectroscopy (EIS) further reveals that CNNO4/PEDOT:PSS exhibits the lowest charge transfer resistance, which is favorable for rapid carrier transport in photovoltaic interfaces. Overall, the electrochemical behavior of these hybrid Dion–Jacobson phase perovskite/PEDOT:PSS materials highlights their potential as electrode candidates for integrated solar water splitting systems and offers valuable insights for designing hybrid perovskite-based energy devices. This study contributes to the development of sustainable and environmentally friendly hydrogen production technologies by enhancing the performance of hybrid electrodes for solar water splitting.

1. Introduction

The advancement of functional materials has emphasized the urgent need for clean energy and efficient energy technologies, as outlined in the United Nations Sustainable Development Goals (SDGs). In particular, SDG 7 encourages affordable and clean energy, SDG 9 promotes Industry, Innovation, and Infrastructure, and SDG 13 focuses on climate action. The development of materials that are both energy-efficient and environmentally friendly is essential for facilitating the transition towards a low-carbon and sustainable global energy system. Therefore, developing

innovative and eco-friendly materials for energy conversion and storage systems has emerged as a primary focus for researchers in the near future.

Among the emerging materials, two-dimensional (2D) materials have emerged as promising candidates for advancing next-generation technologies in diverse fields, such as electronics, optoelectronics, and nanoengineering [1-3]. Their atomic scale thickness and broad lateral size offer opportunities for exploring novel microstructure, physical properties, and innovative functional applications [4]. Dion-Jacobson (DJ) phase perovskite nanosheets have gained significant attention due to their unique structural and functional properties. The DJ phase features a layered structure in which inorganic perovskite slabs are separated by organic spacer cations, forming strong hydrogen bonds that enhance the material's structural stability [5, 6]. These features distinguish DJ perovskites from other layered perovskites, such as the Ruddlesden–Popper phase. Recent studies have explored DJ perovskites in various energy-related applications, including solar cells and light-emitting diodes, highlighting their potential for multifunctional energy systems [7-9].

DJ phase perovskite nanosheets, $Ca_2Na_{n-3}Nb_nO_{3n+1}$ (CNNO), have attracted attention as a promising material due to their controllable layer thickness, strong dielectric response, and notable ferroelectric behavior. Several studies have explored the properties and applications of CNNO nanosheets, which highlight their potential in electrochemical, photovoltaic, and photocatalytic systems. Chang et al. compared molten-salt and solid-state synthesis methods for CNNO (n = 4–6) nanosheets and demonstrated their photoelectrochemical (PEC) hydrogen generation capability, with molten-salt $CNNO_6$ achieving ~0.11% efficiency under UV light [10]. Zhou et al. synthesized the optimized black N/Nb^{4+}-$(Ca_2NaNb_4O_{13})^-$ nanosheets and demonstrated thickness-dependent photocatalytic performance, with the n = 4 variant achieving ~973 μmol h^{-1} hydrogen production when loaded with Pt, emphasizing the critical role of thickness control [11]. Additionally, Osada and Sasaki reviewed DJ-phase perovskites and their exfoliated 2D nanosheets, underlining their notable high-κ dielectric and ferroelectric characteristics, which further support their use in next-generation energy applications [12].

Electrochemical characteristics play a vital role in determining the performance of solar water splitting applications. In these photoelectrochemical devices, materials with high carrier mobility, long charge carrier lifetimes, and low recombination rates are essential to achieve efficient energy conversion [13, 14]. Additionally, materials must exhibit robust redox activity, chemical stability in aqueous environments, and effective interfacial charge transport under illumination. To assess and enhance these properties, techniques like cyclic voltammetry (CV) and electrochemical impedance spectroscopy (EIS) are widely employed.

In our previous works, we evaluated CNNO nanosheets (n = 4–6) as high-κ dielectric electrodes in solar water-splitting cells, reporting a solar-to-hydrogen efficiency of ~0.52% and a hydrogen evolution rate of ~80.6 μmol h^{-1} [15]. Moreover, we revealed a novel mechanism involving photoexcited entangled skyrmions that drive hydrogen evolution, which emphasizes the quantum-level spin-texture contributions to photocatalytic activity [8]. In this research, we aim to deeper investigate the electrochemical characteristics of 2D Dion–Jacobson phase perovskite nanosheets. Through cyclic voltammetry (CV) and electrochemical impedance spectroscopy (EIS), we aim to gain comprehensive insight into charge transfer kinetics, redox behavior, interfacial resistance, and capacitive properties, which enable the rational design of more efficient solar water splitting systems. This hybrid design effectively addresses the inherent limitations of Dion–Jacobson perovskites, such as relatively low electrical conductivity, by integrating them with the conductive polymer PEDOT:PSS to establish efficient charge-transport pathways. This

approach provides a generalizable strategy for engineering multifunctional hybrid electrodes tailored for solar-driven energy conversion.

2. Materials and Methods

2.1 Materials

Potassium carbonate (K_2CO_3) was obtained from Showa Chemical Industry. Sodium carbonate (Na_2CO_3) and a 1.3 wt% aqueous dispersion of poly(3,4ethylenedioxythiophene):poly (styrenesulfonate) (PEDOT:PSS) were obtained from Sigma-Aldrich. Calcium carbonate ($CaCO_3$) and potassium chloride (KCl) were acquired from J. T. Baker. Niobium pentoxide (Nb_2O_5), potassium bicarbonate ($KHCO_3$), and tetrabutylammonium hydroxide (TBAOH; 40 wt% in water) were purchased from Alfa Aesar.

2.2 Methods

To produce 2-D nanosheets from the layered perovskite material $KCa_2Nan_{-3}NbnO_{3n+1}$ (KCNNO), a two-step procedure involving cation-proton exchange followed by exfoliation is required, as shown in Figure 1a. The ion exchange process involves stirring the bulk material in an acidic medium, which replaces the potassium ions (K^+) with protons (H^+) from the solution. After the exchange, exfoliation is achieved by dispersing the protonated product in tetrabutylammonium hydroxide (TBAOH), which infiltrates the interlayer gaps and reduces interlayer bonding, forming unilamellar nanosheets.

Initial materials such as $KCa_2Nb_3O_{10}$ (KCNO) and $NaNbO_3$ (NNO) were synthesized via solid-state reactions at 1473 K. To obtain KCNNO for n = 4, 5, and 6, the two compounds were combined and calcinated at 1573 K for 24 hours in air. The synthesized powder (12.5 g) was then proton-exchanged using 5 M HNO_3 under constant shaking for three days. The resulting product (1.5 g) was exfoliated in 500 mL of TBAOH solution at 270 rpm for seven days. A 1:1 molar ratio of TBA^+ to H^+ was maintained, and centrifugation at 6000 rpm for 30 minutes was applied to remove any unexfoliated residue.

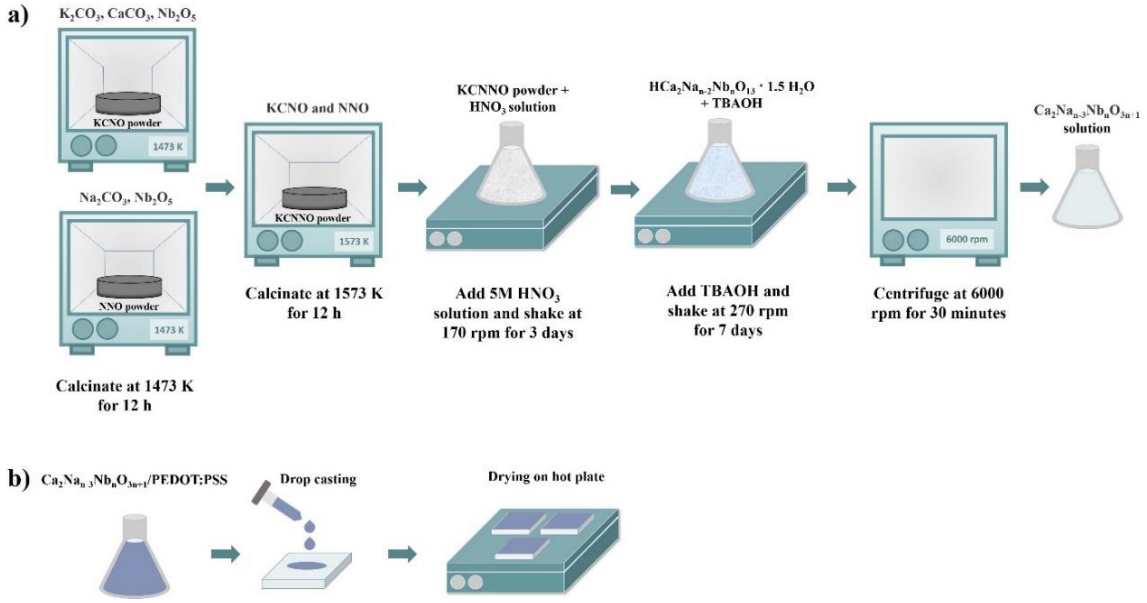

Figure 1. Schematic drawing of (a) CNNO nanosheets synthesis process, and (b) film fabrication process.

A 25 µL mixture of PEDOT:PSS and the $CNNO^-$ colloidal suspension (1:1 ratio) was applied onto a 1 × 1 cm^2 indium tin oxide (ITO) substrate, as shown in Figure 1b. All samples were prepared under identical conditions to ensure consistent film quality, including the amount of solution applied, drying conditions, and equipment used. After deposition, the films were left to stand overnight and then dried at 333 K for one hour. This method ensured the formation of uniform and dense thin films suitable for PEC water splitting applications.

2.3 Electrochemical measurement

The colloidal suspensions were subjected to a transmission electron microscopy (TEM) analysis (FEI EO Tecnai F20 G2 field-emission transmission electron microscope). The cyclic voltammetry (CV) and electrochemical impedance spectroscopy (EIS) characterization were performed using a two-electrode setup, where the $CNNO^-$/PEDOT:PSS sample served as the working electrode, a platinum wire acted as the counter electrode, and 0.5 M $KHCO_3$ aqueous solution was used as the electrolyte. The measurement was conducted using CH instrument.

3. Results and Discussion

3.1 Structural and colloidal characterization of CNNO nanosheets

Figure 2a-c demonstrates the Tyndall effect of $Ca_2Na_{n-1}Nb_nO_{3n+1}$ colloidal suspensions for n=4-6, respectively. The strong Tyndall effect suggests good exfoliation and stable colloidal suspension, which indicates well-dispersed nanosheets. The persistence of the Tyndall effect over time reflects electrostatic stabilization due to surface charges on the nanosheets.

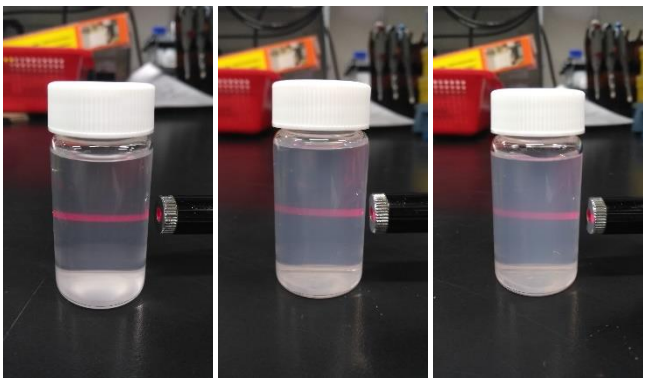

(a) (b) (c)

Figure 2. Tyndall effect of $Ca_2Na_{n-1}Nb_nO_{3n+1}$ colloidal suspensions (a) n=4 (b) n=5, and (c) n=6.

TEM analysis was carried out to examine the morphology of the $Ca_2Na_{n-1}Nb_nO_{3n+1}$ nanosheets. Figure 3 illustrates ultrathin unilamellar nanosheets structures, confirming that the acid-exchange followed by exfoliation process effectively produced well-dispersed 2D perovskite layers.

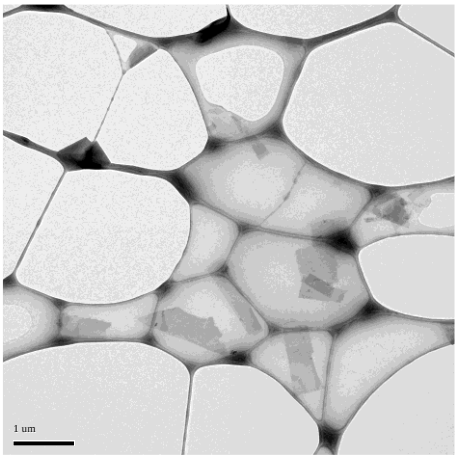

Figure 3. Transmission electron microscope (TEM) images of $Ca_2Na_{n-1}Nb_nO_{3n+1}$ nanosheets.

3.2 Electrochemical characteristics of CNNO/PEDOT:PSS nanosheets

Cyclic voltammetry measurement was conducted to analyze the electrochemical behavior of the samples. The resulting CV curves showed a curved triangle typical of pseudocapacitive behavior, which suggested the presence of quasi-reversible redox reactions occurring between the anodic and cathodic sites, as illustrated in Figure 4a-c. E_{peak} anodic and E_{peak} cathodic refer to the peak currents corresponding to the oxidation and reduction processes, respectively, while E_{onset} anodic and E_{onset} cathodic indicate the initial potentials at which the oxidation and reduction reactions begin, respectively.

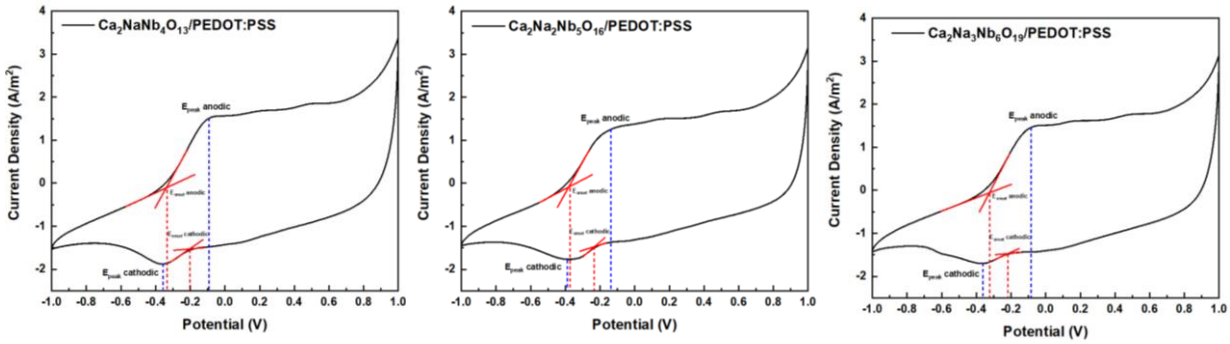

(a) (b) (c)

Figure 4. CV measurement of $Ca_2Na_{n-1}Nb_nO_{3n+1}$/PEDOT:PSS deposited on ITO substrate (a) n=4 (b) n=5, and (c) n=6.

The consistent gap between E_{peak} anodic and E_{peak} cathodic indicates that redox processes maintain good stability. All samples exhibit peak current densities approximately ±2.5–3.5 A/m^2, which suggests significant electrochemical activity. The current density rises as the n values increase, which indicates that the higher n value corresponds to more NbO_6 octahedra slabs, thus the CNNO6 has the highest capability to store charges.

Table 1 demonstrates the CV analysis of CNNO/PEDOT:PSS nanosheets. CNNO5/PEDOT:PSS exhibit the most negative cathodic peak potential (-0.3899 V) and the most negative onset cathodic potential (-0.2330 V), which suggest enhanced electron transfer kinetics compared to the n=4 and n=6 samples. The anodic peak and onset potentials also shift with thickness, with CNNO5/PEDOT:PSS showing a more negative anodic peak (-0.1382 V) and onset (-0.3730 V) than

the other compositions. These variations highlight the critical role of molecular thickness in modulating the redox behavior and, consequently, the electrochemical activity of the CNNO/PEDOT:PSS system.

Table 1. CV analysis of $Ca_2Na_{n-1}Nb_nO_{3n+1}$/PEDOT:PSS deposited on ITO substrate (a) n=4 (b) n=5, and (c) n=6

Sample	E_{peak} anodic (V)	E_{peak} cathodic (V)	E_{onset} anodic (V)	E_{onset} cathodic (V)
CNNO4/PEDOT:PSS	-0.0916	-0.3575	-0.3352	-0.2025
CNNO5/PEDOT:PSS	-0.1382	-0.3899	-0.3730	-0.2330
CNNO6/PEDOT:PSS	-0.0848	-0.3625	-0.3233	-0.2184

Electrochemical impedance spectroscopy measurement was performed to analyze the charge transfer resistance and overall electrochemical performance. Figure 5 shows the Nyquist plot (Z'' vs Z'), which illustrates the impedance response of the electrode in the frequency domain. The semicircle in the initial Nyquist curve indicates the charge transfer resistance.

The addition of the CNNO layer enhances the conductivity compared to pure PEDOT:PSS. Among the samples, CNNO 4 exhibits the most effective charge transfer. However, as the n value rises, the charge transfer resistance also increases, due to the higher ion resistance or structural imbalance.

The sloping line after the semicircle represents the Warburg impedance, which is related to the ion diffusion process in the electrode. PEDOT:PSS exhibits flatter Warburg lines, highlighting slower ion diffusion compared to composites containing CNNO nanosheets. CNNO4 nanosheet shows the lowest charge transport and series resistance, indicating its superior electron and ion transport characteristics.

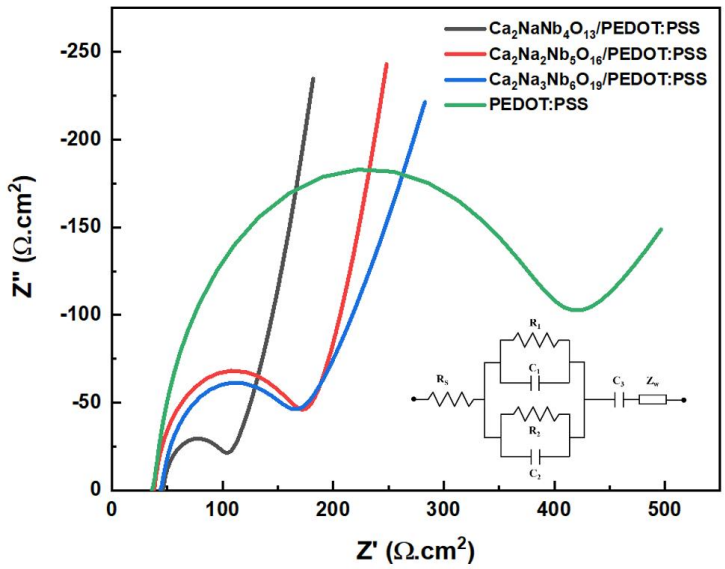

Figure 5. EIS measurement of $Ca_2Na_{n-1}Nb_nO_{3n+1}$/PEDOT:PSS deposited on ITO substrate.

Table 2 summarizes the fitted EIS parameters for each samples, including series resitance (Rs), charge transfer resistances (R_1, R_2), capacitances (C_1, C_2, C_3), and Warburg impedance (Z_t). The CNNO4/PEDOT:PSS sample exhibits a relatively low series resistance (45.80 Ω) and moderate R_1 (48.86 Ω), suggesting efficient charge transport compared to the other composites. The capacitance values (C_1, C_2, C_3) vary significantly among the samples, reflecting differences in their dielectric and interfacial properties. For example, CNNO5/PEDOT:PSS shows a much higher C_1 value (1.05×10^{-5} F) compared to CNNO4/PEDOT:PSS (8.53×10^{-8} F), indicating enhanced charge storage capability.

Based on the provided EIS data, CNNO4/PEDOT:PSS stands out as the best-performing composite for solar water-splitting applications among the tested samples. Its combination of low resistances and balanced capacitance values implies that it can offer enhanced photocurrent generation and reduced energy losses during operation, which are key factors for efficient solar-driven hydrogen production. This aligns with findings in the literature, where materials with optimized impedance characteristics—such as lower charge transfer resistance and suitable capacitance—demonstrate improved PEC water-splitting performance [16]. Therefore, CNNO4/PEDOT:PSS is the most promising candidate for further development in solar water-splitting devices.

Comparing the composites to the pure PEDOT:PSS sample reveals the impact of incorporating $Ca_2Na_{n-1}Nb_nO_{3n+1}$. While PEDOT:PSS alone has the lowest R_s (35.90 Ω), it also displays a much higher R_1 (320.50 Ω), suggesting a higher interfacial resistance. The addition of the perovskite-type oxide phases in the composites generally lowers R_1, which can be attributed to improved interfacial charge transfer. Furthermore, the Warburg impedance (Z_t), which relates to ion diffusion, is slightly higher in the composites, indicating that the presence of the oxide phase may influence ionic mobility. Overall, the EIS analysis demonstrates that the electrical properties of PEDOT:PSS can be tuned by incorporating $Ca_2Na_{n-1}Nb_nO_{3n+1}$, potentially optimizing the material for specific electronic or optoelectronic applications.

Table 2. EIS analysis of $Ca_2Na_{n-1}Nb_nO_{3n+1}$/PEDOT:PSS deposited on ITO substrate.

Sample	R_s (Ω)	R_1 (Ω)	C_1 (F)	R_2 (Ω)	C_2 (F)	C_3 (F)	Z_W (Ω)
CNNO4/PEDOT:PSS	45.80	48.86	8.53×10^{-8}	1.08×10^{8}	8.71×10^{-6}	1.08×10^{-3}	3.24×10^{-3}
CNNO5/PEDOT:PSS	37.62	117.20	1.05×10^{-5}	2.91×10^{8}	8.03×10^{-12}	1.07×10^{-3}	3.02×10^{-3}
CNNO6/PEDOT:PSS	43.67	98.98	7.77×10^{-6}	6.43×10^{8}	2.24×10^{-6}	1.98×10^{-3}	2.01×10^{-3}
PEDOT:PSS	35.90	320.50	1.24×10^{-5}	2.00×10^{9}	2.71×10^{-7}	1.00×10^{1}	2.01×10^{-3}

The apparent discrepancy between the CV and EIS analyses, in which CNNO5/PEDOT:PSS shows the best performance in CV, but CNNO4/PEDOT:PSS shows the best EIS results could be explained by considering the different aspects of electrochemical behavior. CV primarily measures the redox activity and charge storage capacity of the materials, which reflects how efficiently the electrode can undergo reversible oxidation and reduction reactions. The higher redox peak currents and more favorable peak potentials observed for CNNO5/PEDOT:PSS indicate its superior intrinsic electrochemical activity and charge storage capability.

On the other hand, EIS focuses on the resistive and capacitive properties related to charge transport and interfacial processes. The lower series resistance and moderate charge transfer resistance (R_1) of CNNO4/PEDOT:PSS imply that this composite enables more efficient charge transport and less energy loss during operation. Its balanced capacitance values suggest an optimal dielectric and interfacial environment that minimizes recombination and supports steady-state photocurrent generation. This means that although CNNO5/PEDOT:PSS may store more charge and show stronger redox signals, CNNO4/PEDOT:PSS allows charges to move through the system more efficiently, which is critical for continuous solar water splitting under operational conditions.

4. Conclusion

In summary, we have shown the electrochemical characteristics of $Ca_2Na_{n-1}Nb_nO_{3n+1}$/PEDOT:PSS nanosheets through CV and EIS measurements. Both analyses indicate that the addition of CNNO nanosheets into PEDOT:PSS enhances overall performance. Among the three compositions, CNNO5/PEDOT:PSS demonstrates superior redox activity and charge storage capacity, as evidenced by its favorable CV peak potentials and higher current densities. This is beneficial for initial charge accumulation and catalytic processes. However, CNNO4/PEDOT:PSS demonstrated the most efficient charge transport characteristics according to EIS measurements, with a combination of low resistances and well-balanced capacitance values, which suggests its strong potential for effective and improved photocurrent generation by facilitating sustained charge transport and minimizing losses. This research highlights the complementary insights provided by CV and EIS measurement. CNNO5/PEDOT:PSS excels in intrinsic electrochemical activity, whereas CNNO4/PEDOT:PSS offers superior interfacial charge transport and reduced energy losses, both of which are crucial for practical solar water-splitting applications. Overall, CNNO4/PEDOT:PSS emerges as the most promising candidate for integrated solar-driven hydrogen production, combining structural stability, efficient charge transport, and optimized electrochemical properties.

References

[1] A. A. Odebowale et al. 2025. *Micromachines*. **16** 1-28
[2] N. Singh, I. Basumatary, K. C. S. Reddy, and P. Sahatiya. 2025. *Chem. Commun*. **6** 11158-11186
[3] L. M. Shaker, A. A. Abdulamier, and A. A. Al-Amiery. 2025. *J. Alloys Compd*. **1036** 182079
[4] Z. Li et al. 2025. *Nano Energy*. **136** 110719
[5] T. Niu, X. Qifan, and H.-L. Yip. 2021. *Nanophotonics*. **10** 2069-2102
[6] L. Mao et al. 2018. *J Am Chem Soc*. **140** 3775-3783
[7] W. Zhang et al. 2024. *Nat. Commun*. **15** 5709
[8] M. R. Aziza, C.-W. Chang, C.-C. Kaun, and Y.-H. Su. 2021. *J. Phys. Chem. Lett*. **12** 6244-6251
[9] S. Ghimire and C. Klinke. 2021. *Nanoscale*. **13** 12394-12422
[10] C.-W. Chang, A. Nurpratiwi, and S. Yen-Hsun. 2021. *Int. J. Hydrog. Energy*. **47** 40573-40581
[11] Y. Zhou *et al.* 2017. *Chem. - Asian J.*. **12** 2727-2733
[12] M. Osada and T. Sasaki. 2018. *Dalton Trans*. **47** 2841-2851
[13] L. Pan *et al.* 2024. *Nature.* **628** 765-770
[14] Y. Liu *et al.* 2015. *J. Mater. Chem. C.* **3** 12260-12266
[15] M. R. Aziza, C.-W. Chang, A. Mohapatra, C.-W. Chu, C.-C. Kaun, and Y.-H. Su. 2020. *ACS Appl. Nano Mater.* **3** 6367-6375
[16] W. C. Ng and M. N. Chong. 2023. *Sustain. Mater. and Technol.* **38** e00749